ORIGINAL ARTICLE

A more accurate relocation of the 2013 M_s7.0 Lushan, Sichuan, China, earthquake sequence, and the seismogenic structure analysis

F. Long · X. Z. Wen · X. Ruan · M. Zhao · G. X. Yi

Abstract We use a combined earthquake location technique to relocate the M_s7.0 Lushan, Sichuan, China, earthquake sequence of April 20, 2013. A stepwise approach, employing three existing location methods (the HYPOINVERSE method, the Minimum 1-D model, and the Double Difference method), is used to improve location precision by iteratively revising the velocity model station corrections, and hypocenter relocations throughout the process. Our stepwise approach has significantly improved the location precision of the Lushan earthquake sequence, yielding hypocenter locations with final errors of 359, 309, and 605 m in the E-W, N-S, and vertical directions, respectively, with average travel time residuals of 0.12 s. Furthermore, we analyzed the seismogenic structure surrounding the Lushan earthquake sequence by combining the results of the relocated hypocenter distribution with new focal mechanism solutions and information from regional geological and geophysical investigations. From our analysis, we conclude that the vast majority of the aftershocks of the Lushan earthquake sequence occurred at depths of 6–9 km, near the front of the southwestern segment of the NE-trending Longmenshan fault zone. Densely aligned hypocenters clearly suggest that the seismogenic structure of the mainshock consists of a set of basal thrust faults dipping to the NW at 40–50°, at a ramp of the deep basal décollement-thrust system at depths of 7–18 km. Focal mechanism solutions suggest that the seismogenic faults have produced almost pure thrusting. At least one SE-dipping back-thrust is also observed within the basement, as indicated by the hypocenter relocations, which points to either a secondary rupture plane during the mainshock or a plane of aftershock slips. A small number of minor events in the Lushan sequence are located at depths of 0–6 km, with a distribution suggesting that the three NE-trending faults with surface traces running through or passing close to the aftershock area are confined to the upper Mesozoic sedimentary cover, making them independent of the deeper thrust faults that ruptured during the mainshock. Therefore, the 2013 M_s7.0 Lushan earthquake was a blind thrust fault generated on active thrust faults within the basement of the southwestern Longmenshan fault zone, with an upper limit estimation of the rupture length, average down-dip width, and rupture area of 40, 16, and 640 km², respectively.

Keywords Lushan earthquake sequence · High-precision relocation · Combined solution of earthquake location · Error analysis · Seismogenic structure

F. Long (✉) · X. Ruan · M. Zhao · G. X. Yi
Earthquake Administration of Sichuan Province, No. 29, South Renmin Road, section 3, Chengdu 610041 Sichuan, China
e-mail: longfeng1981@gmail.com

X. Z. Wen
State Key Laboratory of Earthquake Dynamics, Institute of Geology, China Earthquake Administration, Yard No.1, Hua Yan Li, Chaoyang District, Beijing 100029, China

1 Introduction

Earthquake location techniques provide an effective way to study the 3-D attitudes of seismogenic structures

from the distribution of accurately located hypocenters of earthquake sequences (Michael 1988; Shearer 1997; Presti et al. 2008). During the period from April 20, 2013, when the M_s7.0 Lushan, Sichuan, China, mainshock occurred, to June 30, 2013, >10,000 aftershocks were recorded. Previous researchers have relocated aftershocks in the early stage of the Lushan earthquake sequence, revealing several features about the seismogenic structure of this earthquake (Fang et al. 2013; Han et al. 2014; Lü et al. 2013; Xu et al. 2013; Zhang and Lei 2013). The primary observation is that the Lushan mainshock likely ruptured one part of the southwestern segment of the NE-trending Longmenshan fault zone, with an epicentral distance ~80 km from the southern end of the 2008 rupture of the M_s8.0 Wenchuan, Sichuan, earthquake (Fig. 1). These previous works have also suggested that the Lushan aftershock zone trends NE-SW (Fig. 1), with the hypocenter of the mainshock being poorly constrained to a depth range of 13–24 km. Inversion

studies targeting the rupture process and focal mechanism solutions of the Lushan earthquake sequence have also illustrated that the Lushan mainshock occurred on a NE-trending thrust fault (Du et al. 2013; Han et al. 2014; Liu et al. 2013b; Lü et al. 2013; Wang et al. 2013a; Xie et al. 2013; Zeng et al. 2013; Zhao et al. 2013). A field survey immediately following the mainshock has verified that no tectonically controlled surface coseismic rupture was produced during the mainshock, leading to the conclusion that the Lushan earthquake occurred on a typical blind reverse-fault (Xu et al. 2013). However, studies of the seismogenic structure of this event have yielded a variety of results, as determined from the relocated hypocenter distributions of early aftershocks of the Lushan sequence using various location methods and velocity models (Fang et al. 2013; Han et al. 2014; Lei et al. 2013; Lü et al. 2013; Xu et al. 2013; Zhang and Lei 2013). These differences are probably due to the complex structure of the southwestern Longmenshan fault zone (Burchfiel et al. 1995, 2008; Xu et al.
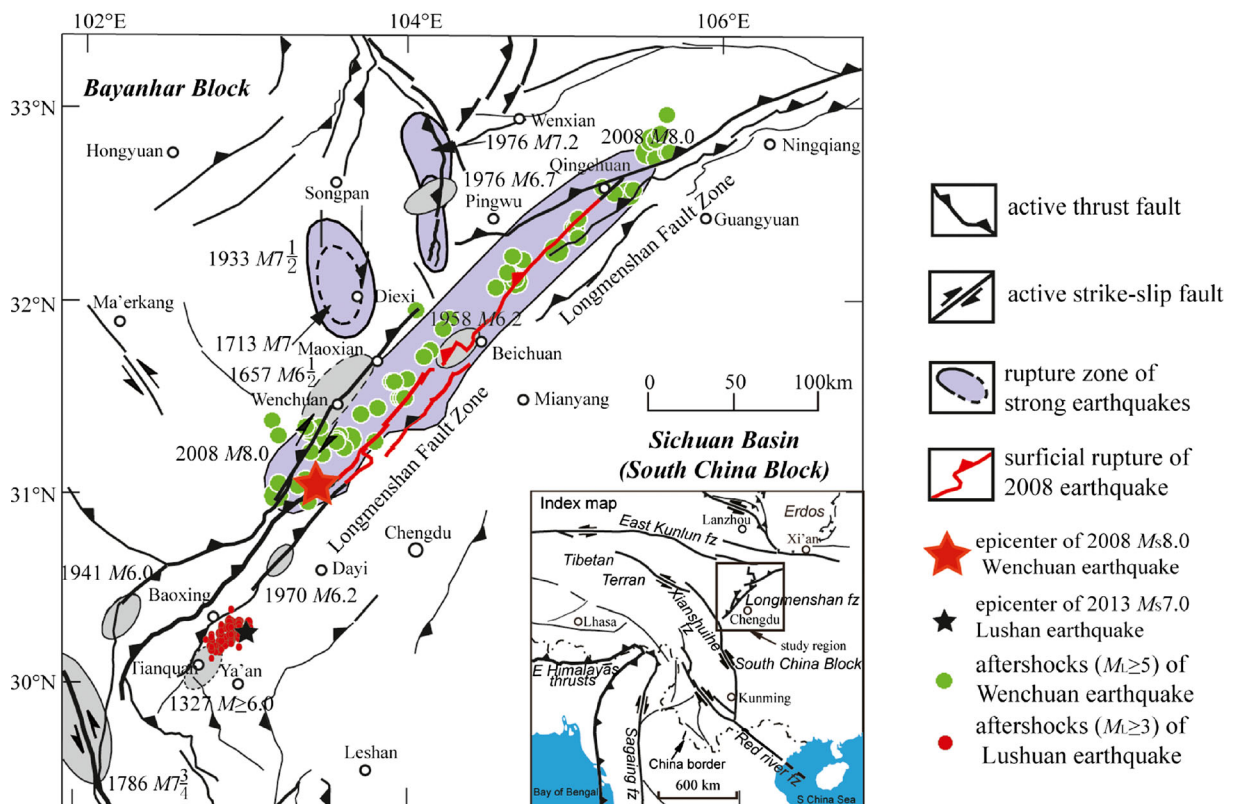

Fig. 1 Map of the Longmenshan fault zone, showing the rupture areas of strong, large historical events and the recent 2008 Wenchuan and 2013 Lushan earthquake sequences. The *inset* gives the location of the study region in relation to the tectonic environment of southwestern China. Aftershock data for the 2008 M_s8.0 Wenchuan and the 2013 M_s7.0 Lushan events were collected on the Sichuan Seismic Network. Faults and earthquake rupture areas are modified from Wen et al. (2009, 2011)

2013), as well as the limited number of aftershocks in the early stage of the earthquake sequence and the limitations of current earthquake-relocation techniques.

In this study, we employ a longer and larger seismic dataset spanning the 2013 Lushan earthquake sequence to improve hypocenter locations and better characterize local seismogenic features. The data used in our relocation approach are evaluated by analyzing the reliability of the relevant seismic records. Based on the existing methods of earthquake relocation, we then search for a technical solution that will effectively improve the location precision.

To date, the general procedure for relocating the Lushan earthquake sequence is as follows. An absolute location method and a regional velocity model are used to obtain an initial location, and a relative location method, such as the Double Difference method (HypoDD; Waldhauser and Ellsworth 2000), is then adopted for the hypocenter relocations (Fang et al. 2013; Lei et al. 2013; Lü et al. 2013; Xu et al. 2013; Zhang and Lei 2013). Such a procedure is simple and fast; however, a well-constrained initial velocity model and/or a rapid evaluation of the earthquake sequence is required. The precision of locations obtained using HypoDD depends on the accuracy of the velocity model (e.g., Michelini and Lomax 2004), as well as the accuracy of the initially located hypocenters (Aster et al. 2005). Thus, an earthquake sequence in a complex tectonic region needs to be carefully analyzed to eliminate the influences of various source errors, and repeat location computations are required, such that a more accurate velocity model is obtained that will yield more accurate earthquake relocations.

Joint velocity modeling and earthquake location techniques provide an effective means of improving the 3-D constraints on seismogenic structures. Chiarabba and Frepoli (1997) combined the VELEST and HYPOINVERSE methods to yield an improved velocity structure (VELEST) and performed a joint earthquake location (HYPOINVERSE) analysis for central and southern Italy. Douilly et al. (2013) used the VELEST method to find the inverse velocity structure and obtain station corrections for the seismogenic zone of the 2010 Haiti earthquake, and then applied the HypoDD method to obtain more accurate earthquake locations for the Haiti sequence. Building from these studies, we adopt a combined earthquake relocation approach, consisting of several established methods that are employed in a stepwise process, with the goal of providing more precise relocations for the 2013 M_s7.0

Lushan earthquake sequence. This revised hypocenter distribution, in combination with focal mechanism solutions, is then analyzed to better characterize the geologic structure of the Lushan seismogenic zone.

2 Seismic data and earthquake location methodology

The precision of earthquake locations is closely related to the distribution of seismic stations, seismic data quality, the velocity model, and the location method. For our relocation of the 2013 Lushan earthquake sequence, seismic data from 12 permanent stations of the Sichuan Seismic Network, 17 stations from three small-aperture networks surrounding local reservoirs (the Zipingpu (ZPP), Pubugou (PBG), and Wawushan (WWS) reservoirs), and 16 portable stations deployed shortly after the Lushan mainshock (Fig. 2a) are analyzed. We focused on relocating those events in the Lushan sequence from the time of the mainshock (April 20, 2013) to June 10, 2013, because a statistical analysis revealed that most of the $M_L \geq 2.0$ events of this sequence occurred during this period (Lei et al. 2013).

To evaluate the data quality and carefully analyze the inversion errors in the location process, we use a combined technique for the relocation, employing three existing seismic location methods in a stepwise procedure, such that the located results from each individual method are evaluated, the corresponding data are updated in time, and a more accurate relocation result is obtained. The technique involves the following steps.

Step 1　Initial earthquake locations are obtained using HYPOINVERSE (Klein 1989). A pre-evaluation of the quality of the relevant seismic data is performed.

Step 2　The seismic data are checked and corrected, if necessary, based on the pre-evaluation in Step 1. We then employ a minimum 1-D model (Kissling 1988; Kissling et al. 1994, 1995) to relocate those events whose seismic data have been checked and corrected, to compute a local 1-D velocity model, and to calculate P wave station corrections from the inversions. This step takes into consideration regions where complicated 3-D velocity structures exist, such as along the Longmenshan fault zone (Wang et al. 2007, 2013b; Zhang et al. 2009), and where large elevation differences exist between
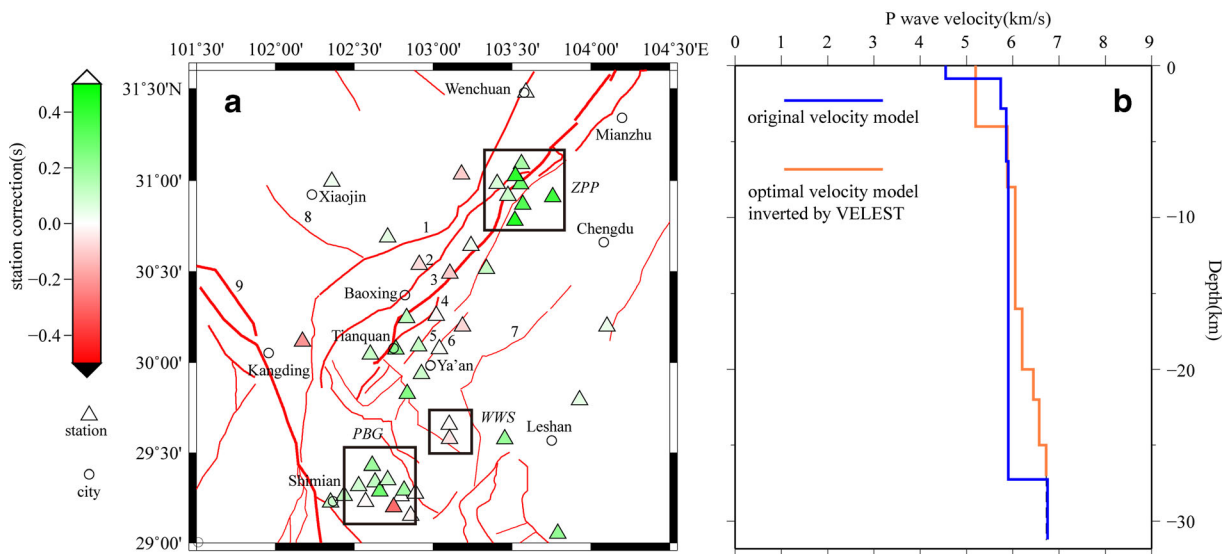
Fig. 2 **a** Map of the seismic network used in this study, with calculated station corrections (delay times). Small-aperture networks were also deployed around the Zipingpu (ZPP), Pubugou (PBG), and Wawashun (WSS) reservoirs, and are outlined by the *three boxes*. Faults of the southwestern Longmenshan fault zone in the study region are numbered as follows: *1* back-range, *2* Baoxing, *3* Shuangshi-Tianqian, *4* Shuangshi-Dachuan, *5* Lushan, *6* Dayi-Mingshan, *7* Xiongpo, *8* Jiajinshan, and *9* Xianshuihe. **b** Initial velocity model (*blue*), from Zhao and Zhang (1987), that was used in Step 1, and the best-fit velocity model (*orange*) from Step 2 of this study

stations (up to 3000 m on either side of the fault zone), both of which affect the earthquake location precision.

Step 3   HYPOINVERSE is run again, using the velocity model, the P wave station corrections, and the location results from Step 2. We then compare the results from Step 3 with the initial results from Step 1 by analyzing the location errors. The aim is to obtain an improved location precision using this method.

Step 4   The location results from Step 3 are used as inputs for the Double Difference method (HypoDD 1.3, http://www.ldeo.columbia.edu/~felixw/hypoDD.html; Waldhauser and Ellsworth 2000; Waldhauser 2001) to obtain a final and more accurate location result.

In the above technique, which employs a multi-method and multi-step location analysis, the location result from each step serves as an input for the next step.

3 Relocation of Lushan earthquake sequence

The multi-method location technique outlined above is applied to the M_s7.0 Lushan, Sichuan, earthquake sequence of 2013. An analysis of several velocity models from the western Sichuan Plateau (e.g., Zhao and Zhang 1987; Wang et al. 2003, 2007, 2013b; Zhang et al. 2009), where we inverted artificial and natural earthquake travel time through each model, led us to choose the Zhao and Zhang (1987) model as our initial velocity model (Fig. 2b). We weighted the data from various seismic stations for the initial location, based on the strong lateral heterogeneity of the crustal structure surrounding the Lushan seismogenic zone and on either side of the Longmenshan fault zone. The relative sizes of these weights depended on the epicentral distance. Stations with epicentral distances of <100 km are given a weight of 1.0. Stations with epicentral distances of 100–150 km are given weights following a cosine function, and those with epicentral distances of >150 km are given a weight of zero. The Step 1 errors for the Lushan sequence location are given in Fig. 3, showing that most locations possess horizontal errors of <2 km and vertical errors of <4 km, with corresponding root-mean-square (RMS) residuals of ≤0.3 s. The data quality of each station-event pair is also checked, where a "station mistake" is defined for $|t_{cal}-t_{obs}| >0.5$ s, and t_{cal} and t_{obs} are the calculated and observed P wave arrival times, respectively. Figure 4 illustrates the station error rates; the maximum error rate of >50 % at station FPO suggests
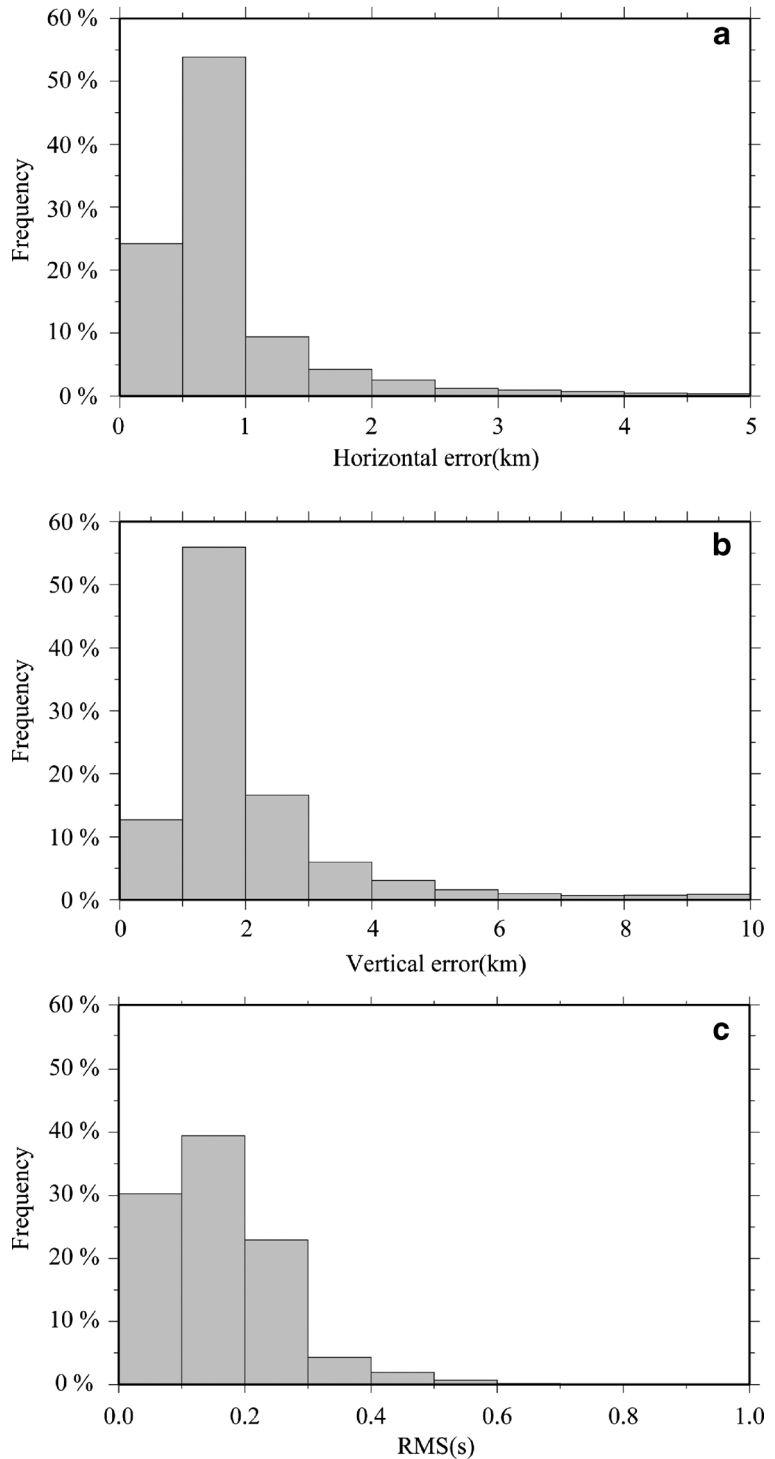
that either inaccurate timing or an incorrect station position may have been used in the initial location of Step 1.

Seismic data from the portable seismic stations deployed only a few days after the mainshock were important in improving the location precision. We investigate the temporal variations in both the average number of stations used in locating each event and the best-fit RMS values at 6-hour intervals in the 6 days

Fig. 4 Distribution of station error rates in Step 1 of the relocation process, for each station used in the analysis possessing >10 seismic records with mistakes
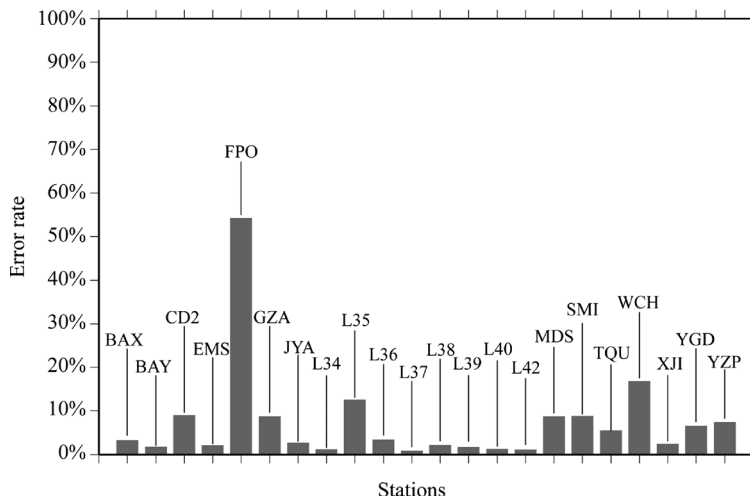
following the mainshock. Figure 5 shows an inverse relationship between the average number of stations and RMS values, whereby an increase in the average number of stations used in the inversion reduced the RMS errors.

Station FPO was removed from the inversion in Step 2 of the relocation process. Still, >24,000 P wave arrivals for 1877 events in the Lushan earthquake sequence were used. Each of the events was recorded at

≥8 stations, with a maximum azimuthal gap of <150° between any two stations. Using the Zhao and Zhang (1987) velocity model (blue line in Fig. 2b) again, we employed the VELEST method (an absolute location method; Kissling 1988), with nine iterations, to obtain an updated relocation catalog of the Lushan earthquake sequence, an optimal 1-D velocity model, and the station delay times. The new velocity model (orange line in Fig. 2b) possesses a more detailed velocity structure
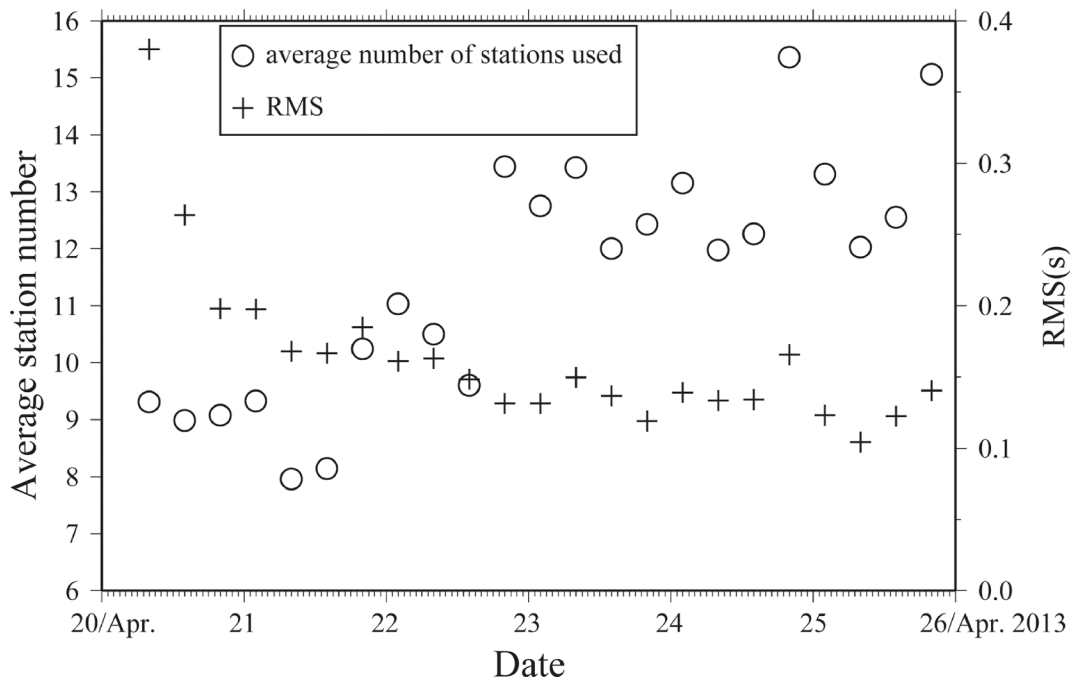

Fig. 5 Temporal variations in the average number of stations used in locating each event and the best-fit RMS values at each time interval. Data are presented every 6 h during the 6 days immediately following the mainshock

than the initial model (blue line in Fig. 2b), particularly within the middle to upper crust. No new velocity structure was determined at >30-km depth since none of the sampled seismic waves traveled through the lower crust. In fact, for stations with epicentral distances of <150 km, only up-going Pg waves can be recorded. Thus, the lower crustal velocity structure of Zhao et al. (2013) is applied to our velocity model, with a Moho depth of 40 km and a corresponding velocity of 7.06 km/s. Station corrections ranged from −0.5 to 0.5 s (Fig. 2a).

The new location results, velocity model, and station delay times from Step 2 then serve as inputs for HYPOINVERSE again to produce revised relocation results in Step 3. Figure 6 demonstrates the improvement in hypocenter relocations from Step 1 to Step 3. The marked decrease in RMS residuals suggests that the travel time errors decreased (Fig. 6a). This is further illustrated by the location error ellipses of 10 $M_L \geq 4.5$ events constrained from Step 1 (solid) and Step 3 (dashed; Fig. 6b). Most of the ellipses from Step 3 shrank relative to those from Step 1, demonstrating that a given event's horizontal position underwent a marked improvement from Step 1 to Step 3. The numbers next to the error ellipses in Fig. 6b indicate differences between the depth errors (in km) from Step 3 and Step 1 for the same 10 events, showing reduced depth errors for 6 of the events.

The final step of the relocation process, Step 4, uses the updated location results and the revised data from Step 3 as inputs for the Double Difference method (HypoDD; Waldhauser and Ellsworth 2000; Waldhauser 2001), to relocate the Lushan sequence again, with HypoDD set to run 12 iterations using a search radius of 3 km. Here, we first relocate all of the events from Step 3 using the LSQR algorithm in HypoDD. We then relocate a subset of 90 events, where all events with $\geq M_L 4.5$ are included and smaller events are randomly selected from the Lushan sequence, using the SVD algorithm in HypoDD. No significant bias between the location results from these two inversion algorithms is observed. We thus chose the results from the LSQR algorithm as our final hypocenter relocations for the Lushan earthquake sequence.

Our final relocation results from Step 4 yield average horizontal locations errors of 359 and 309 m for the E-W and N-S directions, respectively, and an average depth error of 605 m, all with an average RMS of 0.12 s. We also inspect the sensitivity of our final location precision to the hypocentral positions and velocity model used in the location process. We first used the revised hypocentral positions from Step 3 with the initial velocity model (Zhao and Zhang 1987; blue line in Fig. 2b) instead of the revised velocity model from the VELEST algorithm, for the HypoDD relocation analysis. This yielded final average location errors of 520, 813, and 1249 m for the E-W, N-S, and vertical directions, respectively, which are considerably larger than the errors obtained from our stepwise relocation procedure (359, 309, and 605 m). This result shows the importance of the velocity models in minimizing location errors. We then used a dataset of uncorrected hypocentral positions and our original velocity model as inputs for HypoDD, yielding location errors of >1 km. This highlights that the accuracy of the initial hypocentral positions and velocity models have a strong influence on location precision. These two inspections prove that our stepwise earthquake-relocation procedure greatly improves the accuracies of both the initial hypocentral positions and the velocity model, thus minimizing the final location errors.

The location precision of mainshock hypocenters has a strong influence on the analyses that focus on seismogenic structures and coseismic rupture styles. To date, significant differences exist among relocated hypocenter depths of the Lushan mainshock: from the near-real-time reports of 13 and 17 km by the China Seismic Network Center and Earthquake Administration of Sichuan Province, respectively; to 17.4 km by Lei et al. (2013), using HypoDD; to 24 km (http://www.cea-igp.ac.cn/tpxw/266810.shtml), 18 km (Du et al. 2013; Liu et al. 2013b), 16±2 km (Xie et al. 2013), and 14–15 km (Lü et al. 2013), from moment tensor inversions (the CAP method; Zhu and Helmberger 1996); to 12–15 km from rupture process inversions (Liu et al. 2013a; Wang et al. 2013a; Zhang et al. 2013). Using our combined location technique, we also relocated the 2013 $M_s 7.0$ Lushan mainshock. Our result shows that the epicentral position of the mainshock shallowed during the relocation process, and that it was consistently relocated in the 14–16 km depth range in Steps 2–4 (Table 1). Table 1 also illustrates that, from Step 1 to Step 4, the location errors (both position and depth) of the Lushan mainshock are greatly reduced.
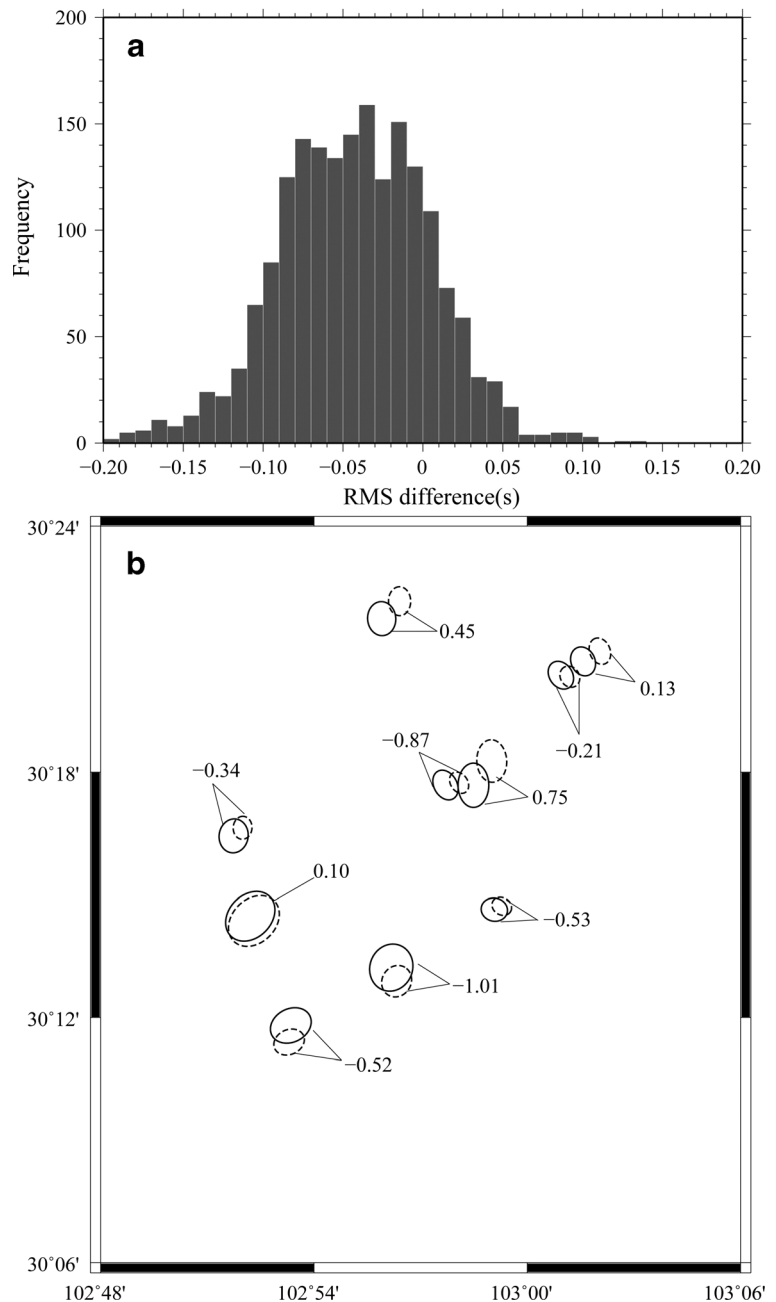
4 Seismogenic structure analysis from relocated hypocenter distribution

4.1 Aftershock distribution and relation to faults

From the final relocation result of the 2013 M_s7.0 Lushan earthquake sequence, we know that the aftershock area covers a ~40-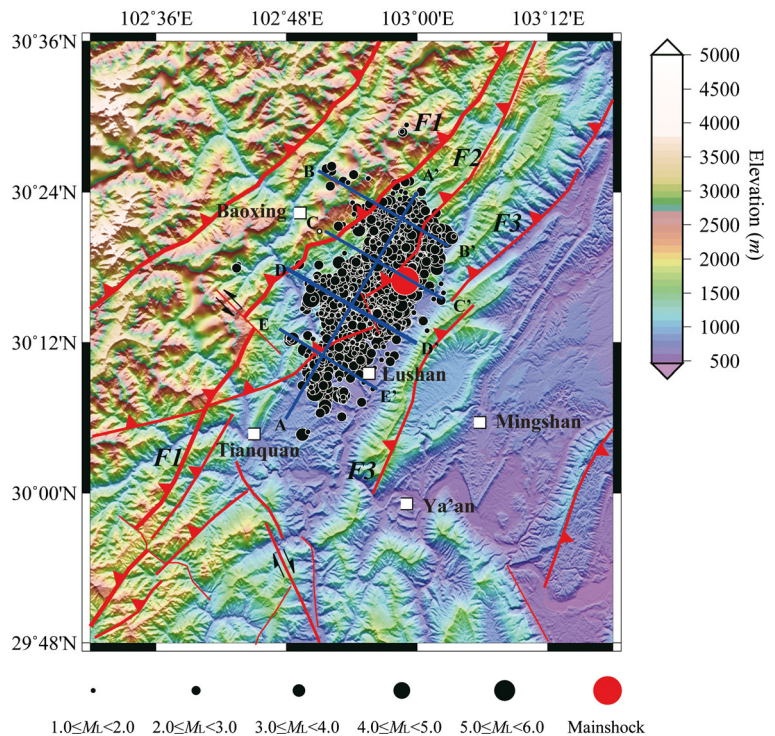km-long section of the southwestern Longmenshan fault zone near Lushan, with a width larger on the northeastern portion than on the southwestern portion. The NE-trending Shuangshi-Dachuan Fault (F2), one of the main branches of the fault zone at the surface, runs through the majority of the aftershock area. The other main branches of the fault zone at the surface, the Shuangshi-Tianqian (F1) and the Dayi-Mingshan (F3) faults, run either side of the aftershock area (Fig. 7).

Table 1 Relocation results from various steps for the M_s7.0 Lushan mainshock of 2013

Step	Location results					
	Time	Epicentral position			Hypocentral depth	
	h m s	Long (°E)	Lat (°N)	Error (km)	Depth (km)	Error (km)
1	08:02:46.75	102.9616	30.2946	0.610	18.71	1.790
2	08:02:46.87	102.9703	30.2982	–	14.71	–
3	08:02:46.97	102.9680	30.2956	0.430	15.59	0.890
4	08:02:47.21	102.9823	30.2821	0.332	14.801	0.338

Previous studies by Zhang and Lei (2013) and Lü et al. (2013) concluded that either F2 or F3 produced the M_s7.0 Lushan earthquake. This conclusion was reached because F2 runs directly through the aftershock area, and the NW-dipping orientation of F3 may extend to the focal depth of the mainshock. However, the poor relocations of the early-stage aftershock distribution led Xu et al. (2013) to infer that the Lushan earthquake occurred along a blind thrust fault. This lack of a definitive source mechanism and location for the 2013 M_s7.0 Lushan earthquake raises the need for better constraints on the structure of the local seismogenic zone.

As shown in Fig. 7, five hypocentral-depth profiles across the aftershock area were made to better delineate the 3-D seismogenic structure of the region. Profile A-A′ is oriented along the strike of the aftershock area, and profiles B-B′, C-C′, D-D′, and E-E′ are oriented perpendicular to the strike of the aftershock area. These profiles are analyzed in detail to define the probable seismogenic structure of the 2013 M_s7.0 Lushan earthquake, using our refined hypocenter relocations in combination with relevant information on the geology and geophysics of the region and new focal mechanism solutions for the mainshock and largest aftershocks in the Lushan sequence (Fig. 8).

4.2 Analysis of seismogenic structure

The vast majority of the relocated hypocenters of the Lushan earthquake sequence occur at depths of 5–19 km (Fig. 8). The northeastern to middle regions of the aftershock area are defined by hypocenters in the 6–19 km depth range, whereas the southwestern region is denoted by a concentration of hypocenters within the 9–15 km depth range. This heterogeneity in seismogenic structure suggests that a geo-structural discontinuity, here labeled d1, exists at a depth of 6–9 km and separates two distinct geological units, here termed the

Fig. 7 Map of the relocated epicenter distribution of the Lushan earthquake sequence. The size of each *circle* is scaled to the magnitude of its representative earthquake. *Red lines* mark active faults in the study region, where *F1*, *F2*, and *F3* represent the Dachuan-Tianquan, Shuangshi-Dachuan, and Dayi-Mingshan faults, respectively. The *blue lines* give the surface positions of the five profiles presented in Fig. 8
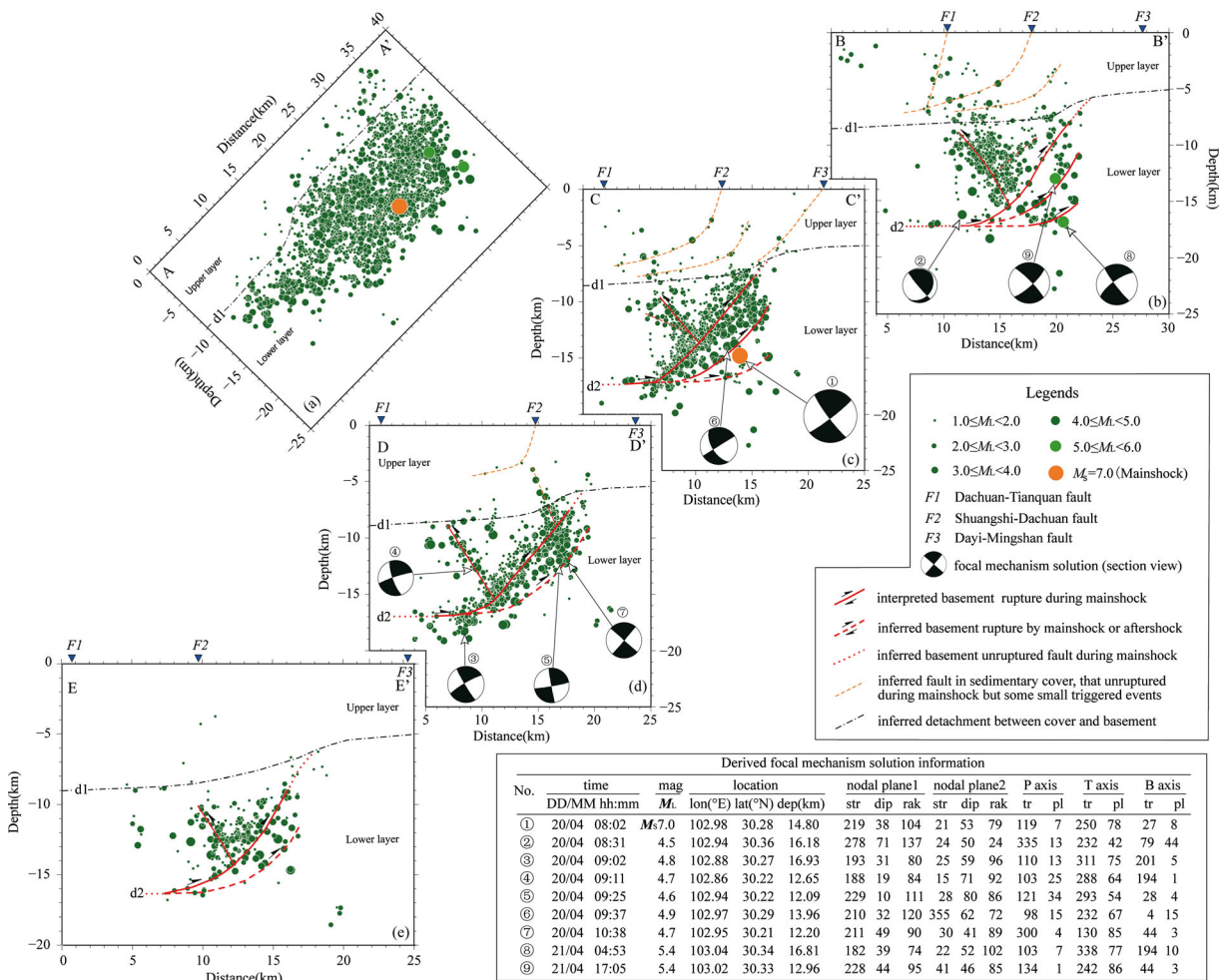
Fig. 8 Profiles highlighting the 2-D depth distribution of the relocated hypocenters for the 2013 Lushan earthquake sequence: **a** A-A′ profile, **b** B-B′ profile, **c** C-C′ profile, **d** D-D′ profile, and **e** E-E′ profile. The surface position of each profile is given in Fig. 7 (*blue lines*). *Circles* mark the relocated hypocenters, scaled by size and color. Focal mechanism solutions were determined for nine events; their solution details are provided in the figure. The *lines* on each profile correspond to various seismogenic structures that have been interpreted from the data. *d1* is interpreted as a discontinuity between two geological units, here labeled *Upper layer* and *Lower layer*. *d2* is interpreted as a deeper basal décollement beneath the Lushan seismogenic zone. The seismogenic zone of the Lushan earthquake sequence is largely confined between d1 and d2. See the text for details

Upper layer and the Lower layer. Since most of the hypocenters are confined to depths below d1, the seismogenic structure of the Lushan earthquake is inferred to exist within the Lower layer.

Recent geological and petroleum-related geophysical surveys have revealed that a basal detachment structure, dipping shallowly to the NW, exists beneath the southwestern Longmenshan fault zone at depths of ~5–8 km near Lushan, extending to the southeast. This structure separates the Upper layer (sedimentary cover composed of deformed Mesozoic units) from the Lower layer (older metamorphic and crystalline basement; Jia et al.

2006; Burchfiel et al. 2008; Zhao et al. 2009). At depth, this low-angle detachment corresponds to the position of the discontinuity d1 in our study (Fig. 8). Furthermore, Lei et al. (2013) proposed that the depth to d1 may delineate the upper surface of a regional Precambrian lithology. These observations suggest that the d1 discontinuity is the décollement between the sedimentary cover and the basement (Fig. 8), in agreement with previous geological and geophysical investigations (Jia et al. 2006; Burchfiel et al. 2008; Zhao et al. 2009). As shown in profiles B-B′ to E-E′ (Fig. 8b–e), the hypocenter distribution of smaller events ($<M_L 3.4$) at

depths of 5–9 km indicates the existence of the d1 discontinuity in some areas from the southeast to the northwest side of the profiles, suggesting that the d1 discontinuity provides an upper limit to the seismogenic structure of the 2013 Lushan earthquake sequence.

However, the abovementioned geological and petroleum-related geophysical investigations (Jia et al. 2006; Burchfiel et al. 2008; Zhao et al. 2009) did not image the deeper structures beneath the d1 discontinuity. On profiles B-B′ to E-E′ (Fig. 8b–e), the distribution of dense hypocenters, including all $M_L \geq 4.0$ aftershocks of the Lushan sequence, clearly delineates two or three NW-dipping (dips of 40–50°) fault planes beneath the d1 discontinuity at depths of 7–18 km. These faults likely ruptured during the mainshock. At depths of 17–18 km, these NW-dipping faults converge upon a nearly horizontal seismogenic zone, d2, that appears to extend farther to the northwest. We infer that d2 is a basal décollement thrust system of the southwestern Longmenshan fault zone. The concentration of earthquake hypocenters along d2 suggests that the Lushan mainshock rupture occurred at a ramp of the deep basal décollement. Furthermore, relatively dense clusters of hypocenters indicate the existence of at least one SW-dipping plane at depths of 8–15 km within the hanging wall of the ruptured NW-dipping faults. This plane may be either a secondary coseismic rupture of the mainshock along a back-thrust fault, or a zone of aftershock slip along the fault. According to the focal mechanism solutions we determined from the CAP method (Zhu and Helmberger 1996; Fig. 8), the mainshock and largest aftershocks of the Lushan sequence resulted from almost pure thrust faulting, with the majority of these solutions possessing NW-dipping nodal planes (Fig. 8b–d). We thus believe that the seismogenic structure of the Lushan earthquake sequence is a NW-dipping thrust system beneath the d1 discontinuity.

It is important to note that two or three NW-dipping fault planes exist within the Lushan earthquake sequence source area, as opposed to a single fault plane (Fig. 8). The relatively dense alignment of hypocenters on profiles B-B′ to E-E′ (Fig. 8b–e) are difficult to explain by coseismic faulting along a single NW-dipping fault plane, whereas faulting along two or three NW-dipping planes provides a more plausible explanation. Cooley et al. (2011) suggested that when a thrust-propagation fold develops, multiple reverse faults are successively produced along the ramp. These faults are sub-parallel, have identical dip directions, and initiate

from an approximately horizontal plane (i.e., a low-angle décollement). These seismogenic features within the Lower layer can thus be explained by the existence of a thrust-propagation fold above the basal décollement, highlighting the structural complexity of the region.

A few small-magnitude ($<M_L 3.4$) earthquakes from the Lushan sequence occurred within the sedimentary cover (Upper layer) above the d1 discontinuity. The alignment of these hypocenters seems to suggest that the three NE-trending faults with surface traces passing through or near the aftershock area (i.e., the Shuangshi-Tianquan (F1), Shuangshi-Dachuan (F2), and Dayi-Mingshan (F3) faults; see Fig. 8) are shallow NW-dipping faults that are confined to the upper sedimentary cover and are independent of the deeper seismogenic structure beneath the d1 discontinuity (Fig. 8). This inference is supported by regional geological and petroleum-related geophysical investigations (Jia et al. 2006; Zhou et al. 2007; Burchfiel et al. 2008; Zhao et al. 2009). This would also explain why no tectonic-controlled coseismic rupture was found along the surface traces of these three faults during the post-seismic field investigation of Xu et al. (2013).

We used the 3-D coverage of the Lushan aftershock zones (Fig. 8) to determine the geometry of the rupture zone for the 2013 Lushan earthquake sequence. We obtained upper limits of the rupture length L and the vertical width h of the rupture to be 40 and 11 km, respectively (A-A′ profile; Fig. 8a). We also estimated the average dip angle α of the rupture planes to be 45° (B-B′ to E-E′ profiles; Fig. 8b–e), and constrained the upper limit of the down-dip width of the general coseismic rupture plane to be $W = h/\cos\alpha \approx 16$ km. This yielded $A = LW = 640$ km^2 at the upper limit of the rupture zone for the 2013 Lushan.

In summary, we conclude that the 2013 $M_S 7.0$ Lushan earthquake was a blind thrust fault beneath the d1 discontinuity, along the southwestern Longmenshan fault zone near Lushan, China. This conclusion is in agreement with Xu et al. (2013), who suggested that the seismogenic structure represents blind reverse faulting. We find no evidence that fault F2 or fault F3 were the seismogenic faults of this earthquake sequence, even though recent studies have hypothesized local reactivation along these shallow fault systems (Lü et al. 2013; Zhang and Lei 2013).

5 Conclusion

We used a combined earthquake location technique to relocate the M_s7.0 Lushan, Sichuan, China, earthquake sequence from April 20 to June 30, 2013. Three earthquake location methods were employed (HYPOINVERSE+VELEST+HypoDD), using a stepwise process to iteratively reduce location errors and effectively improve location precision. Our final result shows that, for the relocated Lushan earthquake sequence, the average location errors are 359, 309, and 605 m in the E-W, N-S, and vertical directions, respectively, with an average RMS of 0.12 s. We obtained a revised epicentral position of 30.2821°N, 102.9823°E for the April 20, 2013 mainshock, with an updated hypocentral depth of 14.8 km. Such robust results demonstrate that this combined location technique is a feasible and effective way to improve the location precision of earthquake sequences.

The improved relocations give new insights on the spatial distribution of events, and thus the seismogenic structure, of the Lushan earthquake sequence. The vast majority of the earthquake aftershocks occurred along and above the basement, at depths of 6–19 km, near the southwestern front of the Longmenshan fault zone. Their distribution provides clear evidence that the seismogenic structure consists of a basal thrust zone, which probably lies at a ramp of the deep basal décollement thrust system. The mainshock appears to have ruptured two or three NW-dipping (dips of 40–50°) thrust faults and concentrated aftershock activity in the 7–18 km depth range; focal mechanism solutions indicate almost pure thrust faulting. At least one SE-dipping back-thrust fault is also observed on the hanging wall of the mentioned ruptured faults, representing either a secondary coseismic rupture during the mainshock or focused aftershock slips. Only a small amount of aftershock events occurred within the sedimentary cover, and their alignment suggests that the three NE-trending faults possessing surface traces within the seismogenic region (i.e., the Shuangshi-Tianquan (F1), Shuangshi-Dachuan (F2), and Dayi-Mingshan (F3) faults) are all NW-dipping faults that are confined to this upper crustal sedimentary cover, and are independent of the basal seismogenic structure. The rupture area of the Lushan earthquake is estimated to be $40×16$ km$=640$ km^2 in size, which, of course, is an upper limit estimate. Therefore, the M_s7.0 Lushan earthquake of 2013 occurred within an active thrust zone in the basement rocks, and resulted from movement upon a blind thrust fault.

References

Aster RC, Borchers B, Thurber CH (2005) Parameter estimation and inverse problems. Elsevier Academic Press, Burlington

Burchfiel BC, Chen Z, Lin Y, Royden LH (1995) Tectonics of the Longmen Shan and adjacent regions, central China. Int Geol Rev 37(8):661–735

Burchfiel BC, Royden LH, Van Der Hilst RD, Hager BH, Chen Z, King RW, Li C, Lü J, Yao H, Kirby E (2008) A geological and geophysical context for the Wenchuan earthquake of 12 May 2008, Sichuan, People's Republic of China. GSA Today 18(7):4–11. doi:10.1130/GSATG18A.1

Chiarabba C, Frepoli A (1997) Minimum 1D velocity models in central and southern Italy: a contribution to better constrain hypocentral determinations. Ann Geofis XL(4):937–954

Cooley MA, Price RA, Dixon JM, Kyser TK (2011) Along-strike variations and internal details of chevron-style, flexural-slip thrust-propagation folds within the southern Livingstone Range anticlinorium, a paleohydrocarbon reservoir in southern Alberta Foothills. Can AAPG Bull 95(11):1821–1849

Douilly R, Haase JS, Ellsworth WL, Bouin MP, Calais E, Symithe SJ, Armbruster JG, de Lepinay BM, Deschamps A, Mildor SL, Meremonte ME, Hough SE (2013) Crustal structure and fault geometry of the 2010 Haiti earthquake from temporary seismometer deployments. Bull Seismol Soc Am 103(4): 2305–2325. doi:10.1785/0120120303

Du F, Long F, Ruan X, Yi GX, Gong Y, Zhao M, Zhang ZW, Qiao HZ, Wang Z, Wu J (2013) The M7.0 Lushan earthquake and the relationship with the M8.0 Wenchuan earthquake in Sichuan, China. Chin J Geophys 56(5):1772–1783. doi:10.6038/cjg20130535, in Chinese with English abstract

Fang LH, Wu JP, Wang WL, Lü ZY, Wang CZ, Yang T, Cai Y (2013) Relocation of the mainshock and aftershock sequences of Ms7.0 Sichuan Lushan earthquake. Chin Sci Bull 58(28–29):3451–3459. doi:10.1007/s11434-013-6000-2

Farr TG, Rosen PA, Caro E, Crippen R, Hensley S, Kobrick M, Paller M, Rodriguez E, Roth L, Seal D, Shaffer S, Shimada J, Umland J, Werner M, Oskin M, Buerbank D, Alsdorf D (2007) The shuttle radar topography mission. Rev Geophys 2007(45):RG2004. doi:10.1029/2005RG000183

Han LB, Zeng XF, Jiang CS, Ni SD, Zhang HJ, Long F (2014) Focal mechanisms of the 2013 Mw 6.6 Lushan, China

earthquake and high-resolution aftershock relocations. Seismol Res Lett 85(1):8–14. doi:10.1785/0220130083

Jia D, Wei GQ, Chen ZX, Li BL, Zeng Q, Yang G (2006) Longmen Shan fold-thrust belt and its relation to the western Sichuan Basin in central China: New insights from hydrocarbon exploration. AAPG Bull 90(9):1425–1447

Kissling E (1988) Geotomography with local earthquake data. Rev Geophys 26(4):659–698

Kissling E, Ellsworth W, Eberhart-Phillips D, Kradolfer U (1994) Initial reference models in local earthquake tomography. J Geophys Res 99:19635–19646

Kissling E, Kradolfer U, Maurer H (1995) VELEST userES guideshort introduction, Tech. rep. Institute of Geophysics, ETH Zurich, kiss@tomo.ig.erdw.ethz.ch

Klein FW (1989) HYPOINVERSE, a program for VAX computers to solve for earthquake locations and magnitudes. U. S. Geological Survey Open-File Report, 89–314, 59 pp

Lei XL, Ma SL, Su JR, Wang XL (2013) Inelastic triggering of the 2013 Mw 6.6 Lushan earthquake by the 2008 Mw7.9 Wenchuan earthquake. Seismol Geol 35(2):411–422. doi:10.3969/j.issn.0253-4967.2013.02.019 (in Chinese with English abstract)

Liu CL, Zheng Y, Ge C, Xiong X, Hsu H (2013a) Rupture process of the Ms7.0 Lushan earthquake, 2013. Sci China Earth Sci 56(7):1187–1192. doi:10.1007/s11430-013-4639-9

Liu J, Yi GX, Zhang ZW, Guan ZJ, Ruan X, Long F, Du F (2013b) Introduction to the Lushan, Sichuan M7.0 earthquake on 20 April 2013. Chin J Geophys 56(4):1404–1407. doi:10.6038/cjg20130434, in Chinese with English abstract

Lü J, Wang XS, Su JR, Pan LS, Li Z, Yin LW, Zeng XF, Deng H (2013) Hypocentral location and source mechanism of the Ms7.0 Lushan earthquake sequence. Chin J Geophys 56(5):1753–1763. doi:10.6038/cjg20130501, in Chinese with English abstract

Michael AJ (1988) Effects of three-dimensional velocity structure on the seismicity of the 1984 Morgan Hill, California, aftershock sequence. Bull Seismol Soc Am 78:1199–1221

Michelini A, Lomax A (2004) The effect of velocity structure errors on double-difference earthquake location. Geophys Res Lett 31. doi:10.1029/2004GL019682

Presti D, Orecchio B, Falcone G, Neri G (2008) Linear versus non-linear earthquake location and seismogenic fault detection in the southern Tyrrhenian Sea, Italy. Geophys J Int 172:607–618

Shearer P (1997) Improving local earthquake locations using the L1 norm and waveform cross correlation: application to the Whittier Narrows, California, aftershock sequence. J Geophys Res 102:8269–8283

Waldhauser F (2001) HypoDD: A computer program to compute double-difference earthquake locations, USGS Open File Rep., 01–113

Waldhauser F, Ellsworth WL (2000) A double-difference earthquake location algorithm: method and application to the northern Hayward fault. Bull Seismol Soc Am 90:1353–1368

Wang CY, Chan WW, Mooney WD (2003) Three-dimensional velocity structure of crust and upper mantle in southwestern China and its tectonic implications. J Geophys Res 108(B9):2442–2459. doi:10.1029/2002JB001973

Wang CY, Han WB, Wu JP, Lou H, Chan WW (2007) Crustal structure beneath the eastern margin of the Tibetan Plateau and its tectonic implications. J Geophys Res 112(B7). doi:10.1029/2005JB003873

Wang WM, Hao JL, Yao ZX (2013a) Preliminary result for rupture process of Apr. 20, 2013, Lushan Earthquake, Sichuan. China Chin J Geophys 56(4):1412–1417. doi:10.6038/cjg20130436 (in Chinese with English abstract)

Wang XL, Ma SL, Guo Z, Lei XL, Xia YJ, Guo X, Yu GZ, Gou XB, Jiang XD (2013b) S-wave velocity of the crust in Three Gorges Reservoir and the adjacent region inverted from seismic ambient noise tomography. Chin J Geophys 56(12):4113–4124. doi:10.6038/cjg20131216 (in Chinese with English abstract)

Wen XZ, Zhang PZ, Du F, Long F (2009) The background of historical and modern seismic activities of the occurrence of the 2008 Ms8.0 Wenchuan, Sichuan, earthquake. Chin J Geophys 52(2):444–454, in Chinese with English abstract

Wen XZ, Du F, Zhang PZ, Long F (2011) Correlation of major earthquake sequences on the northern and eastern boundaries of the BayanHar block, and its relation to the 2008 Wenchuan earthquake. Chin J Geophys 54(3):706–716 (in Chinese with English abstract)

Wessel P, Smith WHF (1991) Free software helps map and display data. Eos Trans AGU 72(441):445–446

Xie ZJ, Jin BK, Zheng Y, Ge C, Xiong X, Xiong C, Hsu H (2013) Source parameters inversion of the 2013 Lushan earthquake by combining teleseismic waveforms and local seismograms. Sci China Earth Sci 56(7):1177–1186

Xu XW, Wen XZ, Han ZJ, Chen GH, Li CY, Zheng WJ, Zhang SM, Ren ZQ, Xu C, Tan XB, Wei ZY, Wang MM, Ren JJ, He ZT, Liang MJ (2013) Lushan Ms7.0 earthquake: a blind reserve-fault event. Chin Sci Bull 58(28–29):3437–3443

Zeng XF, Luo Y, Han LB, Shi YL (2013) The Lushan Ms7.0 earthquake on 20 April 2013: a high-angle thrust event. Chin J Geophys 56(5):1418–1424. doi:10.6038/cjg20130437, in Chinese with English abstract

Zhang GW, Lei JS (2013) Relocations of Lushan, Sichuan strong earthquake (Ms7.0) and its aftershocks. Chin J Geophys 56(5):1746–1771. doi:10.6038/cjg20130534, in Chinese with English abstract

Zhang ZJ, Wang YH, Chen Y, Houseman GA, Tian XB, Wang E, Teng JW (2009) Crustal structure across Longmenshan fault belt from passive source seismic profiling. Geophys Res Lett 36(17):L17310. doi:10.1029/2009GL039580

Zhang Y, Xu LS, Chen YT (2013) Rupture process of the Lushan 4.20 earthquake and preliminary analysis on the disaster-causing mechanism. Chin J Geophys 56(4):1408–1411. doi:10.6038/cjg20130435, in Chinese with English abstract

Zhao Z, Zhang RS (1987) The compilation of regional travel time table in Sichuan. Earthq Res Sichuan 1987(2):29–35 (in Chinese with English abstract)

Zhao Y, Chen W, Xian CL, Cui LJ (2009) A preliminary study on the style of nappe structure on the front of the Longmenshan, western Sichuan. West-china Exploration Engineering, (4):137–139, 143 (in Chinese)

Zhao CP, Zhou LQ, Chen ZL (2013) Source rupture process of Lushan Ms7.0 earthquake, Sichuan, China and its tectonic implications. Chin Sci Bull 58:2444–2450. doi:10.1007/s11434-013-6017-6

Zhou RJ, Li Y, Densmore AL, Ellis MA, He YL, Li YZ, Li XG (2007) Active tectonics of the Longmen Shan region on the eastern margin of the Tibetan plateau. Acta Geol Sin 81(4):593–604

Zhu L, Helmberger DV (1996) Advancement in source estimation techniques using broadband regional seismograms. Bull Seismol Soc Am 86:1634–1641